The Strong CP Problem Solved by Itself Due to Long-Distance Vacuum Effects

Y. Nakamura

RIKEN Center for Computational Science, Kobe, Hyogo, Japan

G. Schierholz

Deutsches Elektronen-Synchrotron DESY, Hamburg

To be sure that your reports and preprints are promptly included in the
HEP literature database
send them to (if possible by air mail):

DESY	DESY
Zentralbibliothek	Bibliothek
Notkestraße 85	Platanenallee 6
22607 Hamburg	15738 Zeuthen
Germany	Germany

The strong CP problem solved by itself due to long-distance vacuum effects

Y. Nakamura[a] and G. Schierholz[b]

[a] RIKEN Center for Computational Science,
Kobe, Hyogo 650-0047, Japan

[b] Deutsches Elektronen-Synchrotron DESY,
22603 Hamburg, Germany

May 5, 2022

Abstract

The vacuum of quantum chromodynamics has an incredibly rich structure at the nonperturbative level, which is intimately connected with the topology of gauge fields, and put to a test by the strong CP problem. We investigate the long-distance properties of the theory in the presence of a topological θ term. This is done on the lattice, using the gradient flow to isolate the long-distance modes in the functional integral measure and tracing it over successive length scales. We find that the color fields produced by quarks and gluons are screened for vacuum angles $|\theta| > 0$, not unexpectedly, thus providing a natural solution of the strong CP problem.

1   Introduction

Quantum chromodynamics (QCD) decribes the strong interactions remarkably well, from the smallest distances probed so far to hadronic length scales where quarks and gluons confine to hadrons. Yet it faces a problem. The theory allows for a CP-violating term S_θ in the action. In Euclidean space-time it reads

$$S_\theta = i\,\theta\,Q\,, \quad Q = \frac{1}{32\pi^2} \int d^4x \; F_{\mu\nu}^a \tilde{F}_{\mu\nu}^a \in \mathbb{Z}\,, \tag{1}$$

where Q is the topological charge, and θ is an arbitrary phase with values $-\pi < \theta \leqslant \pi$. A nonvanishing value of θ would result in an electric dipole moment d_n of the neutron. The current experimental upper limit is $|d_n| < 1.8 \times 10^{-13} e$ fm [1], which suggests that θ is anomalously small. This feature is referred to as the strong CP problem, which is considered as one of the major unsolved problems in the elementary particles field.

It is known from the case of the massive Schwinger model [2] that a θ term may change the phase of the system. Callan, Dashen and Gross [3] have claimed that a similar phenomenon will occur in QCD. The statement is that the color fields produced by quarks and gluons will be screened by instantons for $|\theta| > 0$. 't Hooft [4] has argued that the relevant degrees of

freedom responsible for confinement are color-magnetic monopoles, realized by partial gauge fixing [5], which leaves the maximal abelian subgroup U(1) × U(1) ⊂ SU(3) unbroken. Quarks and gluons have color-electric charges with respect to the U(1) subgroups. Confinement occurs when the monopoles condense in the vacuum, by analogy to superconductivity. This has first been verified on the lattice by Kronfeld *et al.* [6]. In the presence of a θ term the monopoles acquire a fractional color-electric charge proportional to θ, as has been noticed by Witten [7]. It is then expected that the color fields of quarks and gluons will be screened by forming bound states with the monopoles, driving the theory into a Higgs or Coulomb phase [4, 8] for $|\theta| > 0$.

This strongly suggests that θ is restricted to zero in the confining phase of the theory, which would mean that the strong CP problem is solved by itself. A direct derivation of the phase structure of QCD for nonvanishing values of θ from first principles has remained elusive. A crucial step in solving the strong CP problem is to isolate the relevant degrees of freedom. This is a multi-scale problem, which involves the passage from the short-distance weakly coupled regime, the lattice, to the long-distance strongly coupled confinement regime. The framework for dealing with physical problems involving different energy scales is the multi-scale renormalization group (RG) flow. Exact RG transformations are very difficult to implement numerically. The gradient flow [9, 10] provides a powerful alternative for scale setting, with no need for costly ensemble matching. It can be considered as a particular, infinitesimal realization of the coarse-graining step of momentum space RG transformations [11, 12, 13, 14] à la Wilson [15], Polchinski [16] and Wetterich [17], leaving the long-distance physics unchanged, and as such can be used to study RG transformations directly.

In this work we investigate the long-distance properties of the theory in the presence of the θ term (1) using the gradient flow, and show that CP is naturally conserved in the confining phase.

2   The gradient flow

The gradient flow describes the evolution of fields and physical quantities as a function of flow time t. The flow of SU(3) gauge fields is defined by [10]

$$\partial_t B_\mu(t, x) = D_\nu G_{\mu\nu}(t, x), \quad G_{\mu\nu} = \partial_\mu B_\nu - \partial_\nu B_\mu + [B_\mu, B_\nu], \quad D_\mu \cdot = \partial_\mu \cdot + [B_\mu, \cdot], \quad (2)$$

where $B_\mu(t, x) = B_\mu^a(t, x) T^a$, and $B_\mu(t = 0, x) = A_\mu(x)$ is the original gauge field of QCD. It thus defines a sequence of gauge fields parameterized by t. The renormalization scale μ is set by the flow time, $\mu = 1/\sqrt{8t}$ for $t \gg 0$, where $\sqrt{8t}$ is the 'smoothing range' over which the gauge field is averaged. Correlators of the flowed fields are automatically renormalized [18]. The expectation value of the energy density

$$E(t, x) = \frac{1}{2} \operatorname{Tr} G_{\mu\nu}(t, x) G_{\mu\nu}(t, x) = \frac{1}{4} G_{\mu\nu}^a(t, x) G_{\mu\nu}^a(t, x) \quad (3)$$

defines a renormalized coupling

$$g_{GF}^2(\mu) = \frac{16\pi^2}{3} t^2 \langle E(t) \rangle \big|_{t = 1/8\mu^2} \quad (4)$$

at flow time t in the gradient flow (GF) scheme. Varying μ, the coupling satisfies standard (although scheme dependent) RG equations.

For a start we may restrict our investigations to the SU(3) Yang-Mills theory. If the strong CP problem is resolved in the Yang-Mills theory, then it is expected that it is also resolved in QCD. We use the plaquette action [19]

$$S = \beta \sum_{x,\mu<\nu} \left(1 - \frac{1}{3} \operatorname{Re} \operatorname{Tr} U_{\mu\nu}(x)\right) \tag{5}$$

to generate representative ensembles of fundamental gauge fields. For any such gauge field the flow equation (2) is integrated to the requested flow time t. We use a continuum-like version of the energy density $E(t, x)$ obtained from a symmetric (clover-like) definition of the field strength tensor $G_{\mu\nu}(t, x)$ [10]. The simulations are done for $\beta = 6/g^2 = 6.0$ on 16^4, 24^4 and 32^4 lattices. The lattice spacing at this value of β is $a = 0.082(2)$ fm, where we have taken $\sqrt{t_0} = 0.147(4)$ fm to set the scale [20, 21], with t_0 defined by $t_0^2 \langle E(t_0) \rangle = 0.3$. Our current ensembles include 4000 configurations on the 16^4 lattice and 5000 configurations on the 24^4 and 32^4 lattices each. First results on the smaller lattices have been reported in [22].
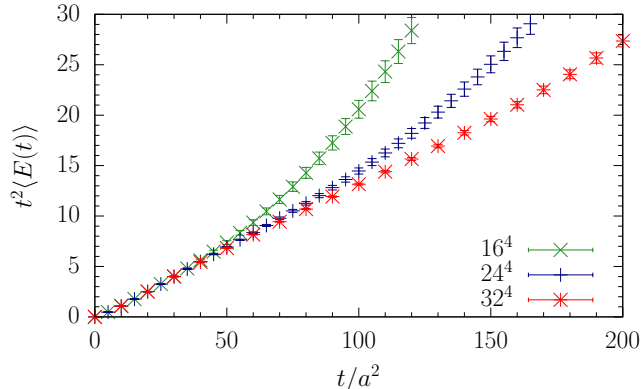

Figure 1: The dimensionless quantity $t^2 \langle E(t) \rangle$ as a function of t/a^2 on the 16^4, 24^4 and 32^4 lattice.

We consider flow times up to $t/a^2 = 200$. This allows us to detect finite size effects, which we expect to show up at $\sqrt{8t} \gtrsim L$, where L is the linear extent of the lattice. In Fig. 1 we show the dimensionless quantity $t^2 \langle E(t) \rangle$ on the 16^4, 24^4 and 32^4 lattice as a function of t/a^2. The data on the 32^4 lattice fall on a straight line up to $t/a^2 \approx 200$, corresponding to $\sqrt{8t} \approx L$. On the 24^4 and 16^4 lattices finite size effects show up at $t/a^2 \approx 100$ and 50, respectively, in rough agreement with $\sqrt{8t} \approx L$. The evaluation of physical quantities will be limited to $t/a^2 \leqslant 100$.

Hadron observables should be independent of the RG scale. In the Yang-Mills theory the choice of observables that can be computed accurately is limited. Two such quantities are the topological susceptibility and the normalized Polyakov loop susceptibility. The topological susceptibility is defined by

$$\chi_t = \frac{\langle Q^2 \rangle - \langle Q \rangle^2}{V}, \tag{6}$$

where $V = L^4$. We define the normalized Polyakov loop susceptibility [23] by

$$\chi_P = \frac{\langle |P|^2 \rangle - \langle |P| \rangle^2}{\langle |P| \rangle^2}, \tag{7}$$

3

where

$$P = \frac{1}{V_3} \sum_{\mathbf{x}} P(\mathbf{x}), \quad P(\mathbf{x}) = \frac{1}{3} \operatorname{Tr} \prod_{x_0=0}^{L-a} U_0(x_0, \mathbf{x}) \tag{8}$$

with $U_0(x_0, \mathbf{x})$ being the (complex valued) link matrix in time direction and V_3 the spatial volume, $V_3 = L^3$. Note that $\langle |P|^2 \rangle$ denotes the Polyakov loop correlator

$$\langle |P|^2 \rangle = \frac{1}{V_3} \sum_{\mathbf{x}} \langle P(0) \, P^\dagger(\mathbf{x}) \rangle. \tag{9}$$

The Polyakov loop requires normalization to be interpreted as the free energy of static quarks. We use the field-theoretic definition (1) of Q. On the 24^4 lattice at flow time $t/a^2 = 50$, for example, the mean deviation from the nearest integer, ΔQ, turns out to be $|\Delta Q/Q| \approx 0.03$ for $|Q| > 0$. In Fig. 2 we show χ_t and χ_P as a function of flow time for $t/a^2 = 10$ to 100. Both quantities are independent of t within the errorbars, as expected. A linear fit to the topological susceptibility gives $\sqrt{t_0}\chi_t^{1/4} = 0.162(3)$. This result agrees precisely with the value reported in [24], $\sqrt{t_0}\chi_t^{1/4} = 0.161(4)$. A linear fit to the Polyakov loop susceptibility gives $\chi_P = 0.289(7)$. We may compare (7) with a 2D Gaussian distribution of real and imaginary P. The outcome is $\chi_P = 4/\pi - 1 = 0.273$, which is close to the lattice result. Later on we shall see that the glueball correlator, respectively the mass gap, is independent of the flow time as well.
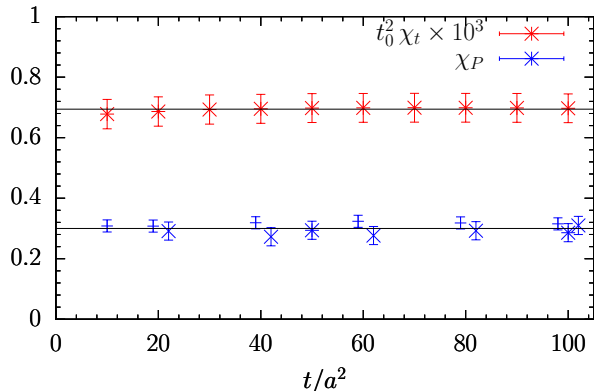

Figure 2: The topological susceptibility χ_t on the 32^4 lattice, and the Polyakov loop susceptibility χ_P on the 16^4 (+), 24^4 (×) and 32^4 (∗) lattice.

It is interesting to note that the field-theoretic definition (1) of Q, where it applies, is independent of the flow time. It is known that the charge density $q = (1/32\pi^2) \, G_{\mu\nu}^a \tilde{G}_{\mu\nu}^a$ can be written as a total derivative, $q = \partial_\mu \omega_\mu$, where ω_μ is the Chern-Simons density or 0-cochain [25]. The latter is gauge variant. Its time derivative, $\partial_t \omega_\mu = (1/8\pi^2) \, \partial_t B_\nu^a \tilde{G}_{\mu\nu}^a$, however is gauge invariant, which leads to $\partial_t Q = 0$ on the periodic lattice after partial integration.

3 Running coupling and linear confinement

The gradient flow running coupling $\alpha_{GF}(\mu) = g_{GF}^2(\mu)/4\pi$, introduced in (4), plays a key role in our investigations. In Fig. 3 we show α_{GF}/π on the 32^4 lattice as a function of $t/a^2 = 1/8\, a^2\mu^2$.
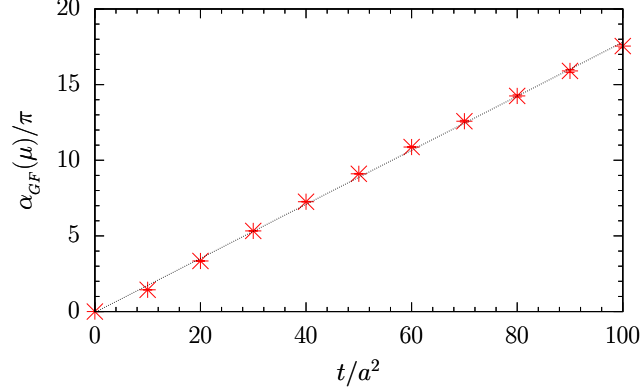
Figure 3: The gradient flow coupling $\alpha_{GF}(\mu)/\pi$ on the 32^4 lattice as a function of $t/a^2 = 1/8a^2\mu^2$, together with a linear fit.

The key result is that α_{GF} is a linear function of $t = 1/8\mu^2$ in the nonperturbative regime. We have already seen that the linear behavior extends to $\sqrt{8t} \approx L$. We can assume that it extends linearly to ever larger values of t as the volume is increased. This results in the gradient flow beta function

$$\frac{\partial\,\alpha_{GF}(\mu)}{\partial\,\ln\mu} \equiv \beta_{GF}(\alpha_{GF}) \underset{\mu \ll 1\,\text{GeV}}{=} -2\,\alpha_{GF}(\mu)\,. \tag{10}$$

For arbitrary values of μ the RG equation (10) has the implicit solution

$$\frac{\Lambda_{GF}}{\mu} = (4\pi b_0\alpha_{GF})^{-\frac{b_1}{2b_0^2}}\exp\left\{-\frac{1}{8\pi b_0\alpha_{GF}} - \int_0^{\alpha_{GF}} d\alpha\,\frac{1}{\beta_{GF}(\alpha)} + \frac{1}{8\pi b_0\alpha^2} + \frac{b_1}{2b_0^2\alpha}\right\}\,, \tag{11}$$

which for large values of t/a^2 leads to

$$\alpha_{GF}(\mu) \underset{\mu \ll 1\,\text{GeV}}{=} \frac{\Lambda_{GF}^2}{\mu^2}\,. \tag{12}$$

A fit of (12) to the lattice data shown in Fig. 3 gives $\sqrt{t_0}\,\Lambda_{GF} = 0.475(16)$.

To make contact with phenomenology, it is desirable to transform the gradient flow coupling α_{GF} to a common scheme. A preferred scheme in the Yang-Mills theory is the V scheme [26]. In this scheme

$$\frac{\Lambda_V}{\mu} = (4\pi b_0\alpha_V)^{-\frac{b_1}{2b_0^2}}\exp\left\{-\frac{1}{8\pi b_0\alpha_V} - \int_0^{\alpha_V} d\alpha\,\frac{1}{\beta_V(\alpha)} + \frac{1}{8\pi b_0\alpha^2} + \frac{b_1}{2b_0^2\alpha}\right\}\,. \tag{13}$$

If we divide Eq. (11) by Eq. (13), we arrive at the relation

$$\frac{\Lambda_{GF}}{\Lambda_V} = \exp\left\{-\int_0^{\alpha_{GF}} d\alpha\,\frac{1}{\beta_{GF}(\alpha)} + \int_0^{\alpha_V} d\alpha\,\frac{1}{\beta_V(\alpha)}\right\}\,. \tag{14}$$

Using (10) and (12), we can solve Eq. (14) for $\beta_V(\alpha_V)$ and $\alpha_V(\mu)$ in the nonperturbative regime. The result is

$$\beta_V(\alpha_V) \underset{\mu \ll 1\,\text{GeV}}{=} -2\,\alpha_V(\mu)\,, \quad \alpha_V(\mu) \underset{\mu \ll 1\,\text{GeV}}{=} \frac{\Lambda_V^2}{\mu^2}\,. \tag{15}$$

5

From the literature we know $\Lambda_V/\Lambda_{\overline{MS}} = 1.600$ [26] and $\Lambda_{\overline{MS}}/\Lambda_{GF} = 0.534$ [10]. This leads to $\sqrt{t_0}\,\Lambda_V = 0.406(14)$ and $\sqrt{t_0}\,\Lambda_{\overline{MS}} = 0.217(7)$. The latter number is in excellent agreement with the outcome of a recent dedicated lattice calculation [27], $\sqrt{t_0}\,\Lambda_{\overline{MS}} = 0.220(3)$.

The linear growth of $\alpha_V(\mu)$ with $1/\mu^2$, which is commonly dubbed infrared slavery, effectively describes many low-energy phenomena of the theory. So, for example, the static quark-antiquark potential, which can be described by the exchange of a single dressed gluon, $V(q) = -\frac{4}{3}\,\alpha_V(q)/q^2$. A popular example is the Richardson potential [28], which reproduces the spectroscopy of heavy quark systems, like charmonium and bottomonium, very well. Upon performing the Fourier transformation of $V(q)$ to configuration space, we obtain

$$V(r) = -\frac{1}{(2\pi)^3}\int d^3\mathbf{q}\; e^{i\,\mathbf{q}\mathbf{r}}\; \frac{4}{3}\,\frac{\alpha_V(q)}{\mathbf{q}^2+i0} \underset{r\gg 1/\Lambda_V}{=} \sigma\, r\,, \tag{16}$$

where σ, the string tension, is given by $\sigma = \frac{2}{3}\Lambda_V^2$. The result is $\sqrt{t_0\,\sigma} = 0.331(11)$. Converted to physical units, we obtain $\sqrt{\sigma} = 445(19)$ MeV, which is exactly what one expects from Regge phenomenology. This gives us confidence in our results, and the linear rise of α_V in particular.
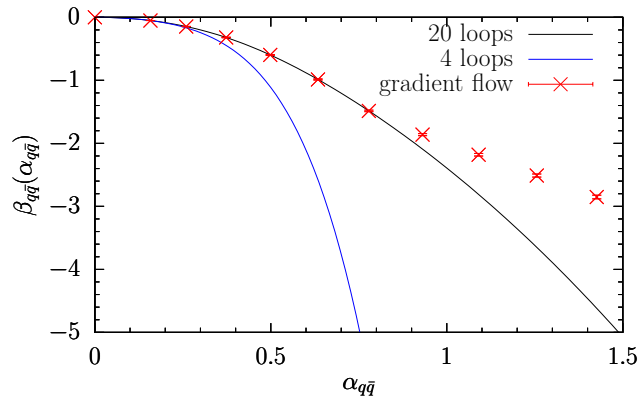

Figure 4: The gradient flow beta function compared to the four-loop and twenty-loop result.

It is interesting to compare the beta function (10), matched to the two-loop result at shorter distances, Eq. (11), with its perturbative counterparts. In Fig. 4 we show the gradient flow beta function, together with the four-loop [29] and twenty-loop [30] perturbative results in the $q\bar{q}$ scheme ($\Lambda_{q\bar{q}}/\Lambda_V = 0.655$). As was to be expected, the perturbative beta function gradually approaches the nonperturbative function with increasing order.

4   Phase structure in the presence of the θ term

With increasing flow time the initial gauge field ensemble splits into effectively disconnected topological sectors of charge Q. This will be the case for ever smaller flow times as the lattice spacing is reduced [10].

We distinguish the topological sectors by the affix Q. The first quantity we look at is the energy density $\langle E(Q,t)\rangle$ in form of the 'action' $S_Q = V\langle E(Q,t)\rangle/8\pi^2$, normalized to one for a single classical instanton. In Fig. 5 we plot S_Q on the 32^4 lattice as a function of t/a^2. While
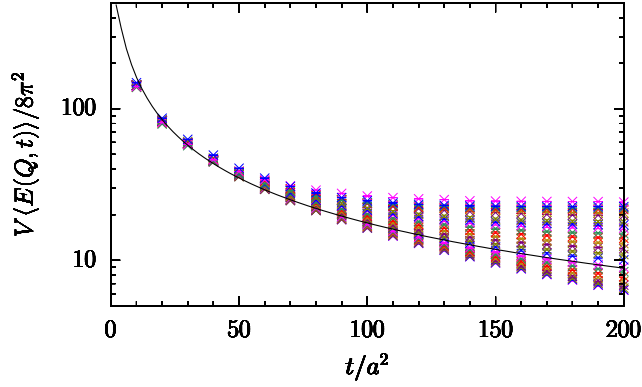
Figure 5: The action $V\langle E(Q,t)\rangle/8\pi^2$ of the different topological sectors as a function of t/a^2 on the 32^4 lattice for charges ranging from $Q = 0$ (bottom) to $|Q| = 22$ (top). The solid line represents the ensemble average. No transition from one sector to the other is observed, in accord with $\partial_t Q = 0$.

$V\langle E(Q,t)\rangle/8\pi^2$ shows a plateau for borderline charges at large flow time, the ensemble average, that is the statistical average across all topological sectors, vanishes like $1/t$.

If the general expectation is correct and the color fields are screened for $|\theta| > 0$, we should find, in the first place, that the running coupling constant will be screened at long distances. From $\langle E(Q,t)\rangle$ we obtain the running coupling $\alpha_V(Q,\mu)$ depending on Q. In Fig. 6 we show $\alpha_V(Q,\mu)$ divided by the ensemble average $\alpha_V(\mu)$ as a function of t/a^2 and Q. Already at relatively small flow times $\alpha_V(Q,\mu)$ starts to fan out according to Q. If multiplied by the lattice volume, the entries of all three figures fall on top of each other. The transformation of $\alpha_V(Q,\mu)$ to the θ vacuum is achieved by the discrete Fourier transform

$$\alpha_V(\theta,\mu) = \frac{1}{Z(\theta)} \sum_Q e^{i\theta Q} P(Q)\, \alpha_V(Q,\mu), \quad Z(\theta) = \sum_Q e^{i\theta Q} P(Q), \tag{17}$$
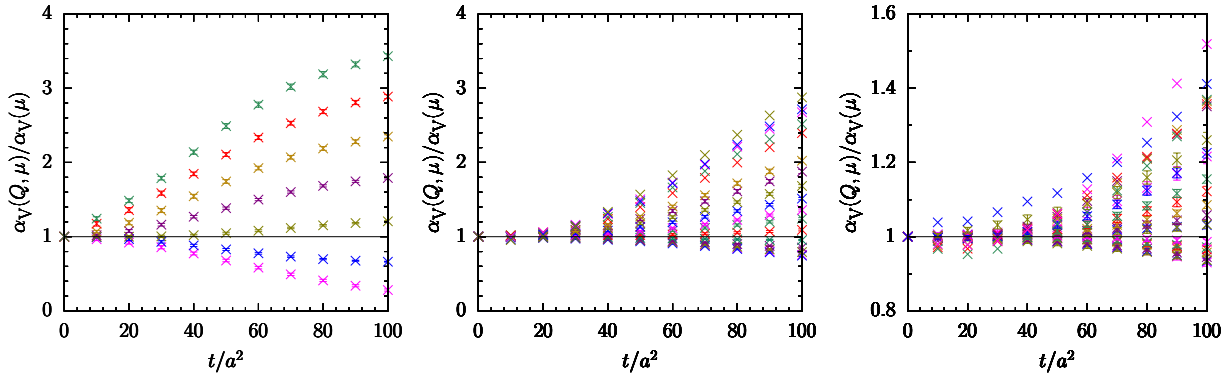

Figure 6: The ratio $\alpha_V(Q,\mu)/\alpha_V(\mu)$ as a function of t/a^2 on the 16^4 (left), 24^4 (center) and 32^4 (right) lattice for charges ranging from $Q = 0$ (bottom) to $|Q| = 6$, 16 and 22 (top), respectively. On the 24^4 and 32^4 lattices no errorbars are shown for marginal values of Q because of limited statistics. On the 16^4 lattice finite volume effects become noticeable for $t/a^2 \gtrsim 50$ ($\sqrt{8t} \gtrsim L$).
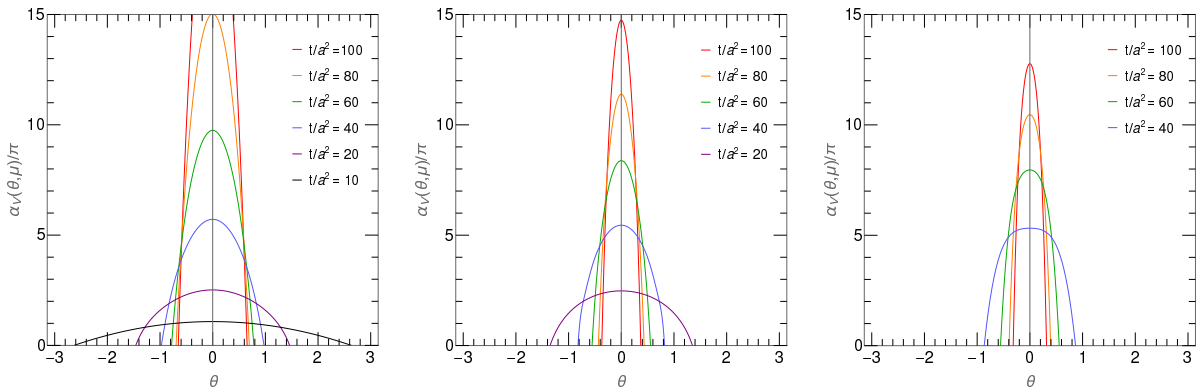
7

Figure 7: The running coupling $\alpha_V(\theta, \mu)$ as a function of θ on the 16^4 (left), the 24^4 (center) and the 32^4 (right) lattice for flow times from $t/a^2 = 10, 20$ and 40 (bottom) to 100 (top), respectively. Note that $\alpha_V \simeq 2.56\, \alpha_{\overline{MS}}$.

where $P(Q)$ is the topological charge distribution at $\theta = 0$ with $\sum_Q P(Q) = 1$. Note that $P(Q)$ is independent of flow time t once the ensemble has settled into disconnected sectors. The partition function is known to be analytic in θ [31, 32]. Limits are set by the precision of $P(Q)$ and $\alpha_V(Q, \mu)$. The statistics needed for consistent precision will increase relatively moderately with the root of the volume. By comparing results on different volumes we can control statistical and systematic effects. We like to emphasize that the transform (17) is not to be viewed as an expansion around the confining vacuum, $\theta = 0$. Rather, it is the weighted average over quantum mechanically disconnected, standalone sectors of the path integral, in which different values of θ label distinct superselection sectors.

We show $\alpha_V(\theta, \mu)$ in Fig. 7 for our three volumes. The leftmost figure indicates finite size effects for $t/a^2 \gtrsim 50$ ($\sqrt{8t} \gtrsim L$) as expected (Fig. 1). We see clearly that the color charge is screened, with the level of screening depending on the scale μ, which specifies the distance, $r \sim 1/\mu$, at which the charge is probed. At large distances the charge appears to be screened for $|\theta| > 0$, while at shorter, perturbative distances the coupling constant becomes gradually independent of θ, reflecting the fact that the θ term is of nonperturbative nature.

Analytically, $\alpha_V(\theta, \mu)$ can be expressed by [22] $\alpha_V(\theta, \mu) = \alpha_V(\mu)\left[1 - \alpha_V(\mu)(D/\lambda)\theta^2\right]^\lambda$, from which derive coupled RG equations. For $\theta^2 \ll 1/\alpha_V(\theta, \mu) \ll 1$ (α_V) and large t (θ), respectively, the equations decouple and reduce to

$$\frac{\partial\left[1/\alpha_V(\theta, \mu)\right]}{\partial \ln t} \simeq -\frac{1}{\alpha_V(\theta, \mu)} + D\theta^2, \quad \frac{\partial \theta}{\partial \ln t} \simeq -\frac{1}{2}\theta. \tag{18}$$

The latter equation has the solution $\theta \propto 1/\sqrt{t}$, which means that θ renormalizes to zero in the infrared limit. In Fig. 8 we show the RG flow of $\pi/\alpha_V(\theta, \mu)$ and θ, with t increasing from top to bottom, for different initial values of θ. The curves are obtained by replacing θ in $\alpha_V(\theta, \mu)$ by $\theta \simeq C/\sqrt{t}$, where C specifies the initial value of θ. The figure shows that confinement implies CP invariance of the strong interactions. An interesting question is if $1/\alpha_V = \theta = 0$ is an IR fixed point of the theory. An analytical derivation of the flow equations would be desirable [33].

Qualitatively similar RG equations for the charge and vacuum angle have been derived from instanton-based models of the vacuum [34, 35]. It thus appears that the renormalization of θ is a
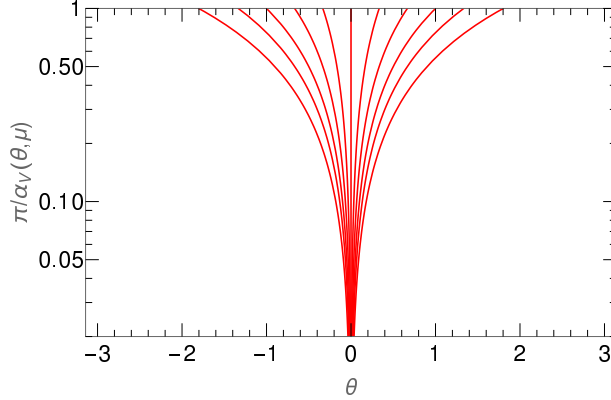
Figure 8: The RG flow of $\pi/\alpha_V(\theta,\mu)$ and θ on the 24^4 lattice for different initial values of θ. Here $D \approx 0.12$ and $\lambda \approx 0.75$.

generic property of instanton fluctuations. Other examples are found in the scaling theory of the integer quantum Hall effect [36], in which the θ angle stands in analogy to the Hall conductivity.

As shown in Fig. 7, screening is a gradual process, which is an important process to understand. Let us stay with the picture of 't Hooft [4], which has been verified in countless publications. (See also the work of [37].) Accordingly, the density of color-electric charge in the θ vacuum is proportional to the density of color-magnetic charge [38, 39, 40] times $|\theta|$. (This appears to be nonperiodic in θ, but this is not so [4].) Thus, the screening length will be the larger the smaller $|\theta|$ is. The result is that at sufficiently long distances (large values of $\sqrt{t}$) the color charge will be totally screened for any $|\theta| > 0$, whereas at shorter distances (smaller values of $\sqrt{t}$) the charge will only be totally screened once the color-electric charge density has reached a sufficiently high level, which requires larger values of $|\theta|$. Below this value the color charge is spatially diluted only, reflected in the parabolic shape of the curves.

The calculations of $\alpha_V(\theta,\mu)$ are rather robust. The determining factor is that $\alpha_V(Q,\mu)$ fans out to a monotonically increasing function of $|Q|$ as t is increased, which makes the numerator of (17) fall off much faster than the denominator, $Z(\theta)$, while the charge distribution $P(Q)$ largely cancels out. An interesting feature of $\alpha_V(\theta,\mu)$ is that for fixed values of $|\theta| > 0$ it rises to a certain point before it drops towards zero as $t = 1/8\mu^2$ is increased. A similar behavior is found for the running coupling $\alpha_s(T,\mu)$ at finite temperature $T > T_c$ [41].

With our current statistics we are not able to compute $\alpha_V(\theta,\mu)$ with confidence for $t/a^2 \lesssim 20$ and 40 on the 24^4 and 32^4 lattice, respectively. But there is no doubt that it will continue to flatten, as seen on the 16^4 lattice. The main hindrance is that fluctuations of $\alpha_V(Q,\mu)$ with respect to Q can be severe on large volumes before the ensemble has settled into truly disconnected topological sectors, as can be seen in Fig. 6. The situation is expected to improve for smaller lattice spacings a.

Let us consider hadron observables now. The Polyakov loop susceptibility, which we considered already in Sec. 2, is a sensitive probe of the long-distance properties of the theory. The Polyakov loop describes a single static quark in the fundamental representation travelling around the periodic lattice. As such, it should be screened for nonvanishing values of θ. We show the bare Polyakov loop correlator $\langle |P|^2 \rangle_Q$ depending on Q as a function of t/a^2 in Fig. 9 (left panel). Also shown is a scatter plot of P at $t/a^2 = 60$ (right panel). Both plots are from the 16^4 lattice,
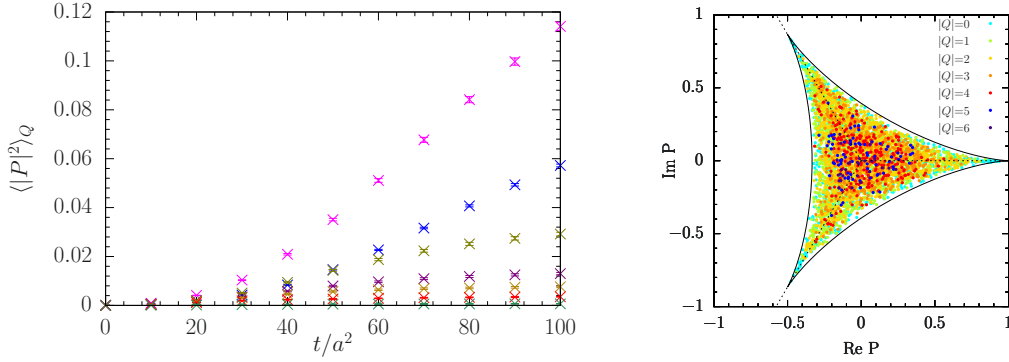
9

Figure 9: Left panel: The Polyakov loop correlator $\langle |P|^2 \rangle_Q$ as a function of t/a^2 for charges ranging from $Q = 0$ (top) to $|Q| = 6$ (bottom). Right panel: The Polyakov loop P for $t/a^2 = 60$ according to charge Q. The data are from the 16^4 lattice.

where we have the largest number of entries per charge. We find $\langle P \rangle = 0$ in each sector. That implies center symmetry for all values of θ. The figure on the right shows that for small values of $|Q|$ the Polyakov loop P rapidly populates the entire theoretically allowed region, while $|P|$ stays small for larger values of $|Q|$. Similar results are found on the larger lattices. In the θ vacuum we have

$$\langle |P|^2 \rangle_\theta = \frac{1}{Z(\theta)} \sum_Q e^{i\theta Q} P(Q) \langle |P|^2 \rangle_Q, \quad \langle |P| \rangle_\theta = \frac{1}{Z(\theta)} \sum_Q e^{i\theta Q} P(Q) \langle |P| \rangle_Q. \qquad (19)$$

From (19) we derive the normalized Polyakov loop susceptibility

$$\chi_P(\theta) = \frac{\langle |P|^2 \rangle_\theta - \langle |P| \rangle_\theta^2}{\langle |P| \rangle_\theta^2}, \qquad (20)$$

which describes the connected part of the Polyakov loop correlator $\langle |P|^2 \rangle_\theta$. We plot the Polyakov loop susceptibility in Fig. 10 for $t/a^2 = 10$ to 100. It shows that the Polyakov loop gets screened, as expected, within a narrow region around $\theta = 0$. Furthermore, the susceptibility is independent
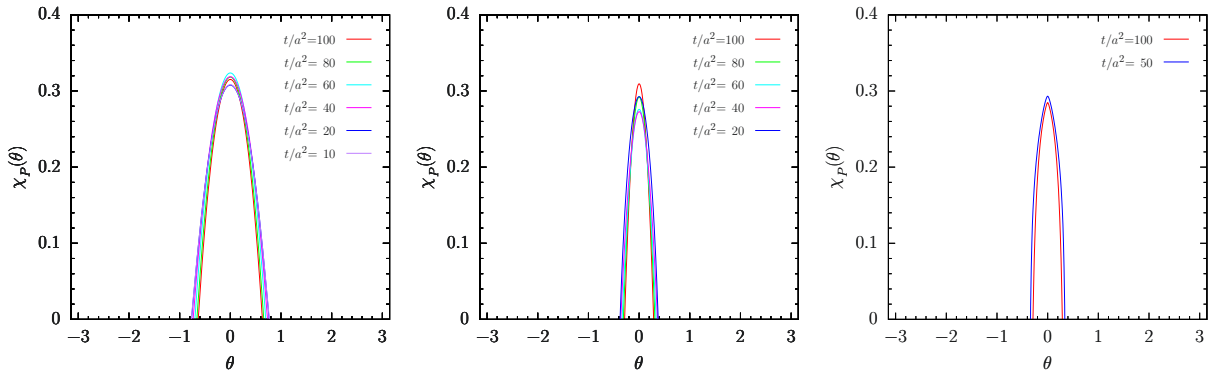

Figure 10: The Polyakov susceptibility $\chi_P(\theta)$ as a function of θ on the 16^4 (left), 24^4 (center) and 32^4 (right) lattice for flow times from $t/a^2 = 10$, 20 and 50 to $t/a^2 = 100$, respectively.

10

of the flow time t, not only for $\theta = 0$, Fig. 2, but for all values of θ. The Polyakov loop is somewhat special, as it can readily be screened by static dyon loops wrapped around the lattice [42, 43].

A further key quantity is the glueball correlator. Above the vacuum, the energy density $E(x,t)$, Eq. (3), projects onto $J^{PC} = 0^{++}$ glueball states. The lowest energy state, which we denote by $m_{0^{++}}$, is called the mass gap. The inverse of the mass gap defines the correlation length, $\xi = 1/m_{0^{++}}$, which describes the length scale over that fluctuations are correlated. The correlation length can be read off from the variance of the energy density, which is identical to the integrated glueball correlator. In the θ vacuum it reads

$$\langle E^2 \rangle_\theta - \langle E \rangle_\theta^2 = \frac{1}{\mathcal{N}} \sum_t \sum_{n>0} |\langle \theta | E | n \rangle|^2 \frac{e^{-m_n t} + e^{-m_n(L-t)}}{2m_n} \simeq \frac{1}{\mathcal{N}} |\langle \theta | E | 0^{++} \rangle|^2 \frac{1}{m_{0^{++}}^2} , \qquad (21)$$

where $\langle E^2 \rangle_\theta = \sum_x \langle E(t,x) E(t,0) \rangle_\theta / V$ and $\mathcal{N} = L^6/16$. (Here t should not be confused with the flow time.) We have assumed that the correlator is dominated by the lowest glueball state. Under the condition that E is normally distributed, it can be shown that the variance is independent of the flow time t. In Fig. 11 we show $\langle E^2 \rangle_{\theta,c} \equiv \langle E^2 \rangle_\theta - \langle E \rangle_\theta^2$ as a function of θ on the 24^4 lattice for three different values of t. As expected, there is little difference between the three curves. Like the Polyakov loop susceptibility, $\langle E^2 \rangle_{\theta,c}$ quickly drops to zero for $|\theta| \gtrsim 0$. Likewise, the correlation length ξ vanishes, most probably in combination with the amplitude $|\langle \theta | E | 0^{++} \rangle|^2$, and the theory has no (finite) mass gap.
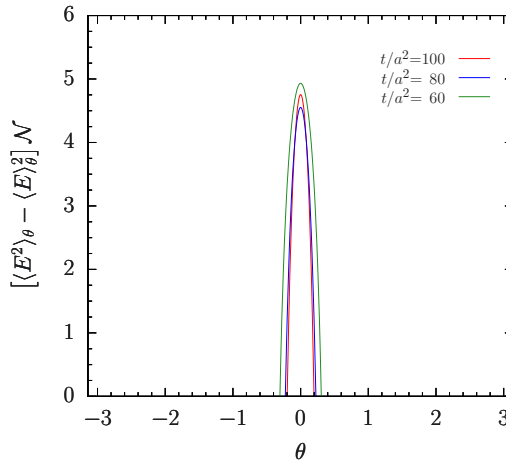

Figure 11: The connected glueball correlator $\langle E^2 \rangle_{\theta,c}$ on the 24^4 lattice as a function of θ for three diferent flow times t.

This raises the question of how the results for $\chi_P(\theta)$ and $\langle E^2 \rangle_{\theta,c}$ fit with the flow of the running coupling $\alpha_V(\theta, \mu)$. While the color charge will eventually be totally screened, and confinement is lost, for $|\theta| > 0$, the situation is different for composite, color-singlet quantities of finite size. Recall that the screening length decreases with increasing value of $|\theta|$, starting from infinity at $\theta = 0$. Thus, for the glueball to dissipate, and the Polyakov loop to be totally screened, the screening length must be smaller than the glueball radius, respectively the radius of the heavy-quark bound state. On the larger lattices this appears to be the case for $|\theta| > 0.2 - 0.3$. The

situation is very similar to the finite temperature phase transition. See, for example, [44]. In that case the screening length depends on the temperature difference $\Delta T = T - T_c$.
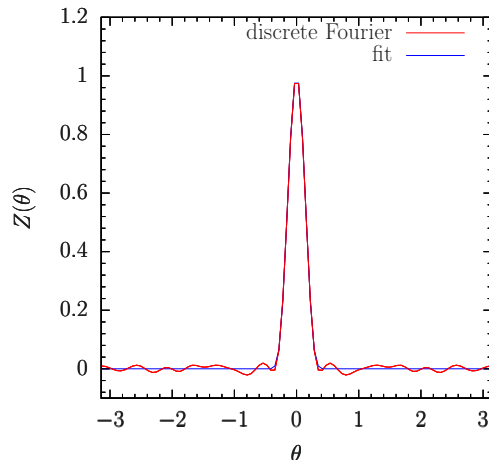

Figure 12: The partition function $Z(\theta)$ on the 32^4 lattice as a function θ, where the discrete Fourier transform, Eq. (17), is compared with a smooth fit.

For the sake of legibility we have not drawn error envelopes in Figs. 7, 10 and 11, as this is the first application of the gradient flow to the infrared behavior of the theory, and we consider it important to clearly display the (in)dependence of the various quantities on t. The running coupling $\alpha_V(\theta, \mu)$, which is the Fourier transform of a convex function, is strictly positive [45]. The Polyakov loop susceptibility $\chi_P(\theta)$ and the variance $\langle E^2 \rangle_{\theta,c}$ are positive by definition. However, after the three quantities have dropped to zero, they start to oscillate around zero with a frequency of $O(|Q|_{\max})$, where $|Q|_{\max}$ is the largest charge being detected, as a result of finite statistics. This is demonstrated in Fig. 12 for the partion function $Z(\theta)$ on the 32^4 lattice. The oscillation amplitude is $\lesssim 0.02$ over the entire range of θ. Various techniques to filter unphysical high-frequency modes from discrete Fourier transforms have been proposed in the literature [46]. We fit the tail of the distributions to a smooth function. Alternatively, one can employ a low-pass filter, like the Savitzky-Golay smoothing filter, which practically gives the same result. With this in mind, we estimate the vertical error in Fig. 7 at 2%, but no smaller than 0.2, and the horizontal error at 10%. In Fig. 10 the vertical error is 6%, but no smaller than 0.02, and the horizontal error is about 15%. In Fig. 11 the vertical error is less than 0.2, and the horizontal error is estimated at 18%.

We may extend the calculation of the static potential in Eq. (16) to nonvanishing, but small values of θ. In this case the θ parameter acts as an infrared cut-off on $\alpha_V(\theta, q)$, which results in $\sigma = 0$ and loss of linear confinement for $|\theta| > 0$.

5 Discussion

The numerical work is characterized by high statistics on three different volumes. A key point is that the path integral splits into disconnected topological sectors. The physics of each sector is classified by the global charge Q only, regardless of whether the simulations started from $\theta = 0$

or from $|\theta| > 0$, which decouples the numerical analysis entirely from θ. The splitting is expected to occur at ever smaller flow times with decreasing value of the lattice spacing. Eventually, the original gauge field ensemble itself will split into disconnected sectors [10]. We found consistent results on all three volumes, which rules out significant systematic and statistical errors. Our main conclusions relate to a very small area of θ around zero only, which does not raise any question of convergence.

The gradient flow proved a powerful tool for tracing the evolution of the gauge field over successive length scales. It passed several tests and showed its potential for extracting low-energy quantities of the theory, highlighted by the topological susceptibility χ_t, the lambda parameter $\Lambda_{\overline{MS}}$ and the string tension σ. As expected, the long-distance properties of the theory remain unchanged under the gradient flow. We can rule out that the vacuum settles to a dilute instanton gas at long distances. In that case $\langle E(t) \rangle \propto 1/\sqrt{V}$, which would lead to $\alpha_{GF} = 0$ in the infinite volume. The novel result is that the color fields produced by quarks and gluons are screened in the θ vacuum by nonperturbative effects, and confinement is limited to $\theta = 0$, which rules out any strong CP violation at the hadronic level. Here screening is a gradual process, characterized by a screening length that decreases with increasing value of $|\theta|$. A similar behavior is found at finite temperatur $T > T_c$. Our results do not come as a surprise [2, 3, 4, 7, 8]. Surprising though is that earlier indications of a nontrivial phase structure have completely been ignored. Probably, because one did not have the tools to address the problem.
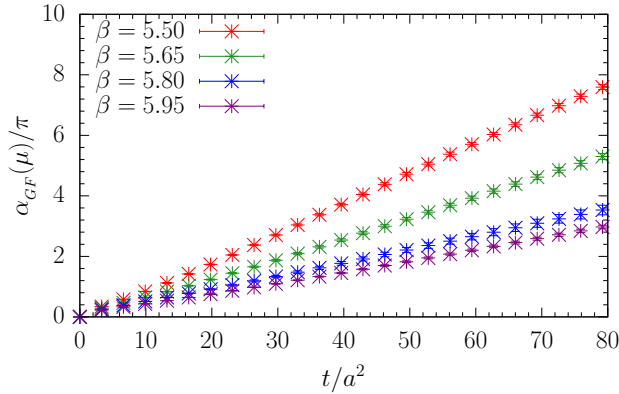

Figure 13: The three-flavor gradient flow coupling $\alpha_{GF}(\mu)/\pi$ for $\beta = 5.50, 5.65, 5.80$ and 5.95 on the $32^3 \times 64$ ($\beta = 5.50$ and 5.65) and $48^3 \times 96$ ($\beta = 5.80$ and 5.95) lattice. The lattice spacings range from $a = 0.074$ to 0.051 fm [20].

Not much changes in three-flavor QCD for heavy quarks. In Fig. 13 we plot $\alpha_{GF}(\mu)$ as a function of t/a^2 at the SU(3) flavor symmetric point [47], $m_\pi = m_K \approx 410$ MeV, for four different values of β. The individual curves fall onto a single straight line when transformed to a common scale. As before, the gauge fields split into disconnected topological sectors at larger flow times. In this case $\Lambda_{\overline{MS}}$ turns out to be close to the quenched value, which is not surprising, given the heavy quark masses. A flavor-diagonal CP-violating phase of the quark mass matrix, which often enters phenomenological estimates of CP violating processes, can always be rotated into a θ term. Hence, the mechanism that screens the color charge in the Yang-Mills theory can be expected to screen the color fields in QCD too.
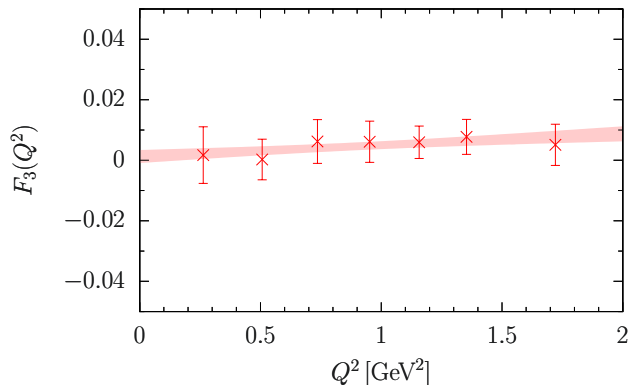
Figure 14: The dipole form factor $F_3(Q^2)$ of the neutron on the $32^3 \times 64$ lattice at the SU(3) flavor symmetric point $m_\pi = m_K = 410\,\mathrm{MeV}$ [20] for $|\theta| \approx 0.4$ and $\beta = 5.50$.

The search for an electric dipole moment of the neutron directly from QCD constitutes a crucial test for our results. If a nonvanishing dipole moment exists, it should be largest for heavy quarks, while it vanishes trivially in the chiral limit. In [48] we have computed $d_n = eF_3(0)/2m_N$ from a fully dynamical simulation of $2 + 1$ flavors of clover fermions including the θ term. The calculation follows [49], corrected for spurious mixing effects of F_3 with the Pauli form factor F_2 [50]. In Fig. 14 we show the dipole form factor F_3 at the SU(3) flavor symmetric point for $|\theta| \approx 0.4$. This leads to $d_n = 0.00028(30)\,[\mathrm{e\,fm}\,\theta]$, which is compatible with zero, as expected. Currently this is the most accurate result. Similar results have been reported in [50, 51, 52], while the authors of [53] claim a nonvanishing value. For small values of θ it can be assumed that the nucleon remains essentially intact. (See above.) In absence of a nonvanishing dipole moment no upper limit of θ can be drawn from the experimental bound on d_n [1]. One might object that EFTs predict a nonvanishing dipole moment for $|\theta| > 0$ [54, 55]. However, there are indications that the chiral condensate $\Sigma(Q)$ grows with a power of $|Q|$ [56, 57, 58], which would lead to $\Sigma(\theta) = 0$ and chiral symmetry restoration for $|\theta| \gtrsim 0$. Under these conditions the predictions of EFTs are no longer tenable. Calculations of $\Sigma(\theta)$ are in progress.

The nontrivial phase structure of QCD has far-reaching consequences for anomalous chiral transformations. Whatever the new phases are, our results are incompatible with the axion extension of the Standard Model. The vacuum will be unstable under the Peccei-Quinn [59] chiral transformation $U_{PQ}(1) = \exp\{i\,\delta Q_5\}$, resulting in the shift symmetry $\theta \to \theta + \delta$, which thwarts the axion conjecture.

Acknowledgment

References

[1] C. Abel *et al.*, Phys. Rev. Lett. **124** (2020) 081803 [arXiv:2001.11966 [hep-ex]].

[2] S. R. Coleman, Annals Phys. **101** (1976) 239.

[3] C. G. Callan, R. F. Dashen and D. J. Gross, Phys. Rev. D **20** (1979) 3279.

[4] G. 't Hooft, Nucl. Phys. B **190** (1981) 455.

[5] A. S. Kronfeld, G. Schierholz and U. J. Wiese, Nucl. Phys. B **293** (1987) 461.

[6] A. S. Kronfeld, M. L. Laursen, G. Schierholz and U. J. Wiese, Phys. Lett. B **198** (1987) 516.

[7] E. Witten, Phys. Lett. B **86** (1979) 283.

[8] J. L. Cardy and E. Rabinovici, Nucl. Phys. B **205** (1982) 1.

[9] R. Narayanan and H. Neuberger, JHEP **0603** (2006) 064 [hep-th/0601210].

[10] M. Lüscher, JHEP **1008** (2010) 071 [Erratum: JHEP **1403** (2014) 092] [arXiv:1006.4518 [hep-lat]].

[11] M. Lüscher, PoS LATTICE **2013** (2014) 016 [arXiv:1308.5598 [hep-lat]].

[12] H. Makino, O. Morikawa and H. Suzuki, PTEP **2018** (2018) 053B02 [arXiv:1802.07897 [hep-th]].

[13] Y. Abe and M. Fukuma, PTEP **2018** (2018) 083B02 [arXiv:1805.12094 [hep-th]].

[14] A. Carosso, A. Hasenfratz and E. T. Neil, Phys. Rev. Lett. **121** (2018) 201601 [arXiv:1806.01385 [hep-lat]].

[15] K. G. Wilson and J. B. Kogut, Phys. Rept. **12** (1974) 75.

[16] J. Polchinski, Nucl. Phys. B **231** (1984) 269.

[17] J. Berges, N. Tetradis and C. Wetterich, Phys. Rept. **363** (2002) 223 [arXiv:hep-ph/0005122 [hep-ph]].

[18] M. Lüscher and P. Weisz, JHEP **02** (2011) 051 [arXiv:1101.0963 [hep-th]].

[19] K. G. Wilson, Phys. Rev. D **10** (1974) 2445.

[20] V. G. Bornyakov, R. Horsley, R. Hudspith, Y. Nakamura, H. Perlt, D. Pleiter, P. E. L. Rakow, G. Schierholz, A. Schiller, H. Stüben and J. M. Zanotti, [arXiv:1508.05916 [hep-lat]].

[21] N. Miller, L. C. Carpenter, E. Berkowitz, C. C. Chang, B. Hörz, D. Howarth, H. Monge-Camacho, E. Rinaldi, D. A. Brantley and C. Körber, C. Bouchard, M. A. Clark, A. S. Gambhir, C. J. Monahan, A. Nicholson, P. Vranas and A. Walker-Loud, Phys. Rev. D **103** (2021) 054511 [arXiv:2011.12166 [hep-lat]].

[22] Y. Nakamura and G. Schierholz, PoS LATTICE **2019** (2019) 172 [arXiv:1912.03941 [hep-lat]].

[23] A. Bazavov, N. Brambilla, P. Petreczky, A. Vairo and J. H. Weber, Phys. Rev. D **98** (2018) 054511 [arXiv:1804.10600 [hep-lat]].

[24] M. Cè, C. Consonni, G. P. Engel and L. Giusti, Phys. Rev. D **92** (2015) 074502 [arXiv:1506.06052 [hep-lat]].

[25] M. L. Laursen, G. Schierholz and U. J. Wiese, Commun. Math. Phys. **103** (1986) 693.

[26] Y. Schröder, Phys. Lett. B **447** (1999) 321 [arXiv:hep-ph/9812205 [hep-ph]].

[27] M. Dalla Brida and A. Ramos, Eur. Phys. J. C **79** (2019) 720 [arXiv:1905.05147 [hep-lat]].

[28] J. L. Richardson, Phys. Lett. B **82** (1979) 272.

[29] M. Donnellan, F. Knechtli, B. Leder and R. Sommer, Nucl. Phys. B **849** (2011) 45 [arXiv:1012.3037 [hep-lat]].

[30] R. Horsley, H. Perlt, P. E. L. Rakow, G. Schierholz and A. Schiller, Phys. Lett. B **728** (2014) 1 [arXiv:1309.4311 [hep-lat]].

[31] C. Vafa and E. Witten, Phys. Rev. Lett. **53** (1984) 535.

[32] M. Aguado and M. Asorey, AIP Conf. Proc. **1343** (2011) 173; M. Aguado, M. Asorey and D. Garcia-Alvarez, Mod. Phys. Lett. A **18** (2003) 2303.

[33] H. Suzuki, private communication.

[34] C. G. Callan, R. F. Dashen and D. J. Gross, Phys. Rev. D **17** (1978) 2717.

[35] V. G. Knizhnik and A.Y. Morozov, JETP Lett. **39** (1984) 240 [Pisma Zh. Eksp. Teor. Fiz. **39** (1984) 202].

[36] H. Levine, S. B. Libby and A. M. M. Pruisken, Phys. Rev. Lett. **51** (1983) 1915 [Erratum: Phys. Rev. Lett. **52** (1984) 1254]; H. Levine and S. B. Libby, Phys. Lett. B **150** (1985) 182.

[37] N. Seiberg and E. Witten, Nucl. Phys. B **426** (1994) 19 [Erratum: Nucl. Phys. B **430** (1994) 485] [arXiv:hep-th/9407087 [hep-th]].

[38] V. Bornyakov and M. Müller-Preussker, Nucl. Phys. B Proc. Suppl. **106** (2002) 646 [arXiv:hep-lat/0110209 [hep-lat]].

[39] V. G. Bornyakov, H. Ichie, Y. Koma, Y. Mori, Y. Nakamura, D. Pleiter, M. I. Polikarpov, G. Schierholz, T. Streuer, H. Stüben and T. Suzuki, Phys. Rev. D **70** (2004) 074511 [arXiv:hep-lat/0310011 [hep-lat]].

[40] M. Hasegawa, JHEP **09** (2020) 113 [arXiv:1807.04808 [hep-lat]].

[41] F. M. Steffens, Braz. J. Phys. **36** (2006) 582 [arXiv:hep-ph/0409329 [hep-ph]].

[42] V. Bornyakov and G. Schierholz, Phys. Lett. B **384** (1996) 190 [arXiv:hep-lat/9605019 [hep-lat]].

[43] M. L. Laursen and G. Schierholz, Z. Phys. C **38** (1988) 501.

[44] T. Matsui and H. Satz, Phys. Lett. B **178** (1986) 4162.

[45] E. Tuck, Bulletin of the Australian Mathematical Society **74(1)** (2006) 133.

[46] W. H. Press, S. A. Teukolsky, W. T. Vetterling and B. P. Flannery, *Numerical Recipes: the Art of Scientific Computing*, Cambridge University Press (Cambridge, 2017).

[47] W. Bietenholz, V. Bornyakov, M. Göckeler, R. Horsley, W. G. Lockhart, Y. Nakamura, H. Perlt, D. Pleiter, P. E. L. Rakow, G. Schierholz, A. Schiller, T. Streuer, H. Stüben, F. Winter and J. M. Zanotti, Phys. Rev. D **84** (2011) 054509 [arXiv:1102.5300 [hep-lat]].

[48] M. Batelaan, F. K. Guo, U. G. Meißner, Y. Nakamura, G. Schierholz, J. M. Zanotti *et al.*, "The electric dipole moment of the neutron from 2+1 flavor lattice QCD: an update", in preparation.

[49] F. K. Guo, R. Horsley, U.-G. Meissner, Y. Nakamura, H. Perlt, P. E. L. Rakow, G. Schierholz, A. Schiller and J. M. Zanotti, Phys. Rev. Lett. **115** (2015) 062001 [arXiv:1502.02295 [hep-lat]].

[50] M. Abramczyk, S. Aoki, T. Blum, T. Izubuchi, H. Ohki and S. Syritsyn, Phys. Rev. D **96** (2017) 014501 [arXiv:1701.07792 [hep-lat]].

[51] C. Alexandrou, A. Athenodorou, K. Hadjiyiannakou and A. Todaro, Phys. Rev. D **103** (2021) 054501 [arXiv:2011.01084 [hep-lat]].

[52] T. Bhattacharya, V. Cirigliano, R. Gupta, E. Mereghetti and B. Yoon, Phys. Rev. D **103** (2021) 114507 [arXiv:2101.07230 [hep-lat]].

[53] J. Dragos, T. Luu, A. Shindler, J. de Vries and A. Yousif, Phys. Rev. C **103** (2021) 015202 [arXiv:1902.03254 [hep-lat]].

[54] R. J. Crewther, P. Di Vecchia, G. Veneziano and E. Witten, Phys. Lett. B **88** (1979) 123 [Erratum: Phys. Lett. B **91** (1980) 487].

[55] F. K. Guo and U.-G. Meissner, JHEP **12** (2012), 097 [arXiv:1210.5887 [hep-ph]].

[56] D. Diakonov, Proc. Int. Sch. Phys. Fermi **130** (1996) 397 [arXiv:hep-ph/9602375 [hep-ph]].

[57] T. Schäfer and E. V. Shuryak, Rev. Mod. Phys. **70** (1998) 323 [arXiv:hep-ph/9610451 [hep-ph]].

[58] E. Follana, A. Hart, C. T. H. Davies and Q. Mason Phys. Rev. D **72** (2005) 054501 [arXiv:hep-lat/0507011 [hep-lat]].

[59] R. D. Peccei and H. R. Quinn, Phys. Rev. Lett. **38** (1977) 1440; Phys. Rev. D **16** (1977) 1791.

[60] Y. Nakamura and H. Stüben, PoS **LATTICE2010** (2010) 040 [arXiv:1011.0199 [hep-lat]].

[61] T. R. Haar, Y. Nakamura and H. Stüben, EPJ Web Conf. **175** (2018) 14011 [arXiv:1711.03836 [hep-lat]].